The effect of bullet yaw on the threat level; a numerical investigation

K. Tomczyk[1], D. Landheer[1], T. Williams[1], S. Bailey[2], V. Skelton[2], J. Warnett[3], A. Attridge[3], M. A. Williams [3]

[1]*Simpact Engineering Ltd., 5 Benford Court, Lower Cape, Warwick, CV34 5DA, United Kingdom, karol.tomczyk@simpact.co.uk, tel.: +44 (0)1926 498620*
[2]*Morgan Advanced Materials, Composites and Defence Systems, 473 Foleshill Road, Coventry, CV6 5AQ, United Kingdom*
[3]*WMG, University of Warwick, CV4 7AL, United Kingdom*

Abstract. It is well known that yaw can affect the penetrative power of armour piercing rounds. To investigate this effect purely experimentally is difficult because the typical ballistic set up does not allow control over the yaw angle of the projectile. In this study, a numerical model is used complementing ballistic experiments for a range of yaw angles. For the projectile, a validated computer model of the 30-06 7.62 x 63mm AP M2 round was selected. Surrogate targets were used for a qualitative assessment of the phenomenon. The utilized target is a flat rectangular tile. To encourage yaw in the experimental tests, targets were positioned at relatively close distance to the breach and impact velocity was chosen lower than typical for the projectile. Both ensure that the bullet does not reach stable flight therefore yaw is present. From the experiments, a range of impact velocities and yaw angles was chosen and each of the test conditions simulated. The decrease in bullet velocity ΔV was calculated from high speed video footage captured during tests and compared to bullet ΔV in simulation. Strain condition, predicted damage and negative pressure output from simulation were investigated in pursue of yaw effects on threat level. The results of this study can help in the interpretation of physical test results and ultimately can contribute to making the performance of armour systems more robust.

1. INTRODUCTION

The work described in this paper makes use of the output generated from an ongoing 2 year Technology Strategy Board (TSB) funded collaborative Research and Development project 'Transforming the Role of Simulation in New Product Development' which the authors of this paper have been involved in.

The effect of the orientation of a bullet at time of first contact with hard armour on its threat level is the subject of this paper. Bullet orientation at any moment in time can be described by three angles, the bullet yaw, pitch and roll angle. Roll is the rotation around the symmetry axis of the bullet. The roll angle does not change the geometry of the impact condition, as bullets are typically approximately rotation symmetric. The resultant angle of yaw and pitch is also referred to as 'Yaw'. In this study we focus on events where the centre of gravity of the bullet travels in a straight line and 'Yaw' is the angle measured between bullet direction of travel and the symmetry axis of the bullet. In scenarios where the target is perpendicular to the direction of flight of the projectile, 'no yaw' implies that the first point of contact is in line of flight of the centre of gravity of the projectile. This means that no kinetic energy is converted into rotational energy in case of a symmetric target response. One could conclude that this gives the highest penetrative power. However, our experiments indicate that the presence of a small amount of yaw can reduce the velocity drop of bullet heads shot through identical (ceramic) targets. The same phenomenon is reported in literature [1].

In scenarios where the target is not perpendicular to the direction of flight of the projectile, i.e.: small angles of obliquity a similar effect is reported [2].

It is suspected that tangent contact load components affect the damage initiation in the target. The authors use a combination of experiments and numerical simulation to investigate these effects. For this work the 30-06 7.62 x 63mm AP M2 armour piercing bullet is selected as projectile because of its relatively good consistency and the fact that it is used in armour standards. Commonly available 95% Al2O3 ceramic tiles are used as targets.

2. THREAT

2.1 30-06 7.62 x 63mm AP M2

The AP-M2 used for this research is a 7.62 x 63mm armour piercing round having approximately 10.5g of mass as measured for the purposed of this paper which corresponds to the average mass measured by [3]. For this work it was decided that it would be best to use a threat that was manufactured as consistently as possible in order to minimise experimental variance coming from the round itself. The projectile is defined as a reference round in the widely acknowledged National Institute of Justice standard for its level IV protection level. All rounds used for these experiments came from the same batch; a selection of bullets from this batch was sectioned and hardness tested. **Figure 1** shows a sectioned bullet sample with the micro Vickers points. Because most of the damage occurs in the tip of the bullet it was looked into in detail. Hardness measurements at the centre of steel core were done as well and showed hardness value in the range of 600 – 650 HV, similar to the values recorded for the tip.

The hardness results for this sample are given in **Table 1**. Based on the hardness measurements, an approximate tensile strength of 1850 MPa for steel core was assumed for the FEA simulation model.

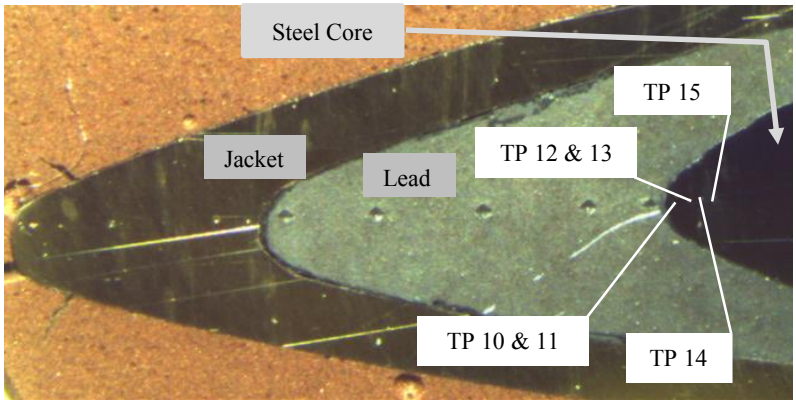

Figure 1. Sectioned bullet sample for hardness testing

Table 1. Vickers hardness measurements of steel core (penetrator) tip

Measurement	TP10&11	TP12&13	TP14	TP15	Average	Std. dev.
Vickers Hardness	558	615	579	607	590	26

The obtained steel core hardness results are approximately 250 HV less than reported in [3]. In [3] the location of the measurement points is not detailed, possibly measurements were taken from the steel core surface. Measurements on the outer surface can give higher readings. In the current research the hardness was measured on sectioned cores as shown on **Figure 1**, an area judged representative for our modelling purposes.

2.2 CT scanning

The geometry of the projectile consists of the brass jacket and end cap, the steel penetrator and lead tip ballast. In order to determine the representative local jacket thicknesses, in particular at the tip of the projectile, X-ray computed tomography was applied. A detailed description of the process of X-ray CT characterisation of bullets geometries can be found in [4]. The same method can also be used to accurately measure post impact dimensions on the damaged projectile [5]. **Figure 2** shows an image of the 3D post impact X-ray CT of a damaged AP-M2. Clearly visible are the distorted jacket with rifle marks and the penetrator showing a fracture surface where the tip is missing.

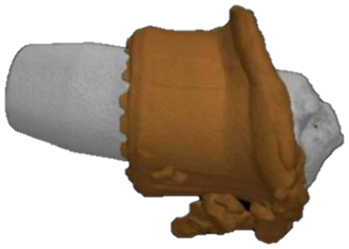

Figure 2. X-ray CT image of a damaged AP M2.

3. BALLISTIC TESTING

Ballistic testing was carried out to compliment and substantiate the numerical studies. This was carried out at the Morgan Advanced Materials 15 m development range in Coventry.

Around 20 AP-M2 bullet heads were fired from a remote breach perpendicularly into flat square ceramic alumina tiles measuring 100 mm x 100 mm x 8 mm. The AP-M2 bullet heads were acquired from FN Herstal, Belgium. For modelling simplicity, these were unconstrained but simply supported on one edge on a flat platform for centre impact by the incoming round. The powder in the casing was measured to give impact velocities of the order of around 400-500 m/s. This was the calculated velocity range where the highest practical frame rate could be used to measure round velocity and yaw from High Speed Video (HSV) footage with good accuracy (±30 m/s and ±1° respectively). A lower than normal impact velocity for the projectile encourages yawing and to further promote a yawing round, the sample was positioned 5m from the breach. At this relatively close distance the round does not reach stable flight. Therefore, the test set-up ensured that the threat yaws upon reaching the target.

A schematic of the experimental setup is shown in **Figure 3**. A pair of Photron SA High Speed Video (HSV) cameras were mounted directly overhead the ceramic sample so that the left and right camera produced a perpendicular view of the incoming and exiting round respectively. These were both protected by a single layer of transparent polycarbonate sheet. A frame rate of 100,000 fps and a resolution of 320 x 128 pixels for both gave a practical view of the incoming and exiting round. The unit on the left was used to confirm round incoming velocity given by the range chronograph before impact and also the yaw of the bullet around the vertical and horizontal axes. By making use of a rectangular mirror adjacent to the impacting bullet, it was also possible to calculate yaw of the bullet around the horizontal axis. As the majority of the projectiles remained intact, a 'bullet catcher' was constructed from a rigid steel framework supporting several single layers of Dyneema used to decelerate each bullet with minimal further damage.

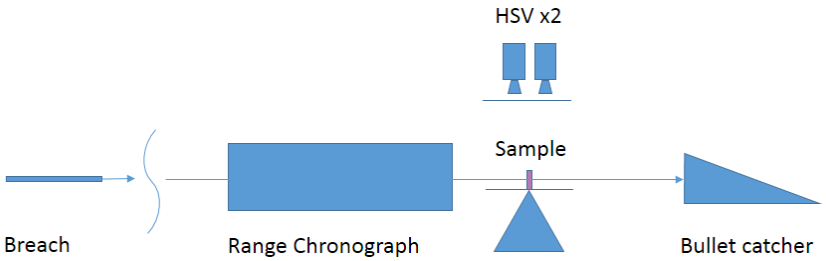

Figure 3. Schematic of test set-up in the Morgan range

Figure 4 shows the views from the HSV units. Self-adhesive measurement tape was stuck to the platform in each test as a reference for the position of the bullet with respect to time. The image on the left shows the yawing round of Test 13 at the point where the tip contacts the surface of the ceramic tile. Directly above the measurement tape is the rectangular mirror in which you can see the yaw of the round in the horizontal axis. The image on the right shows the debris field where the exit velocity of the projectile is identified (circled in red) and exit velocity calculated.

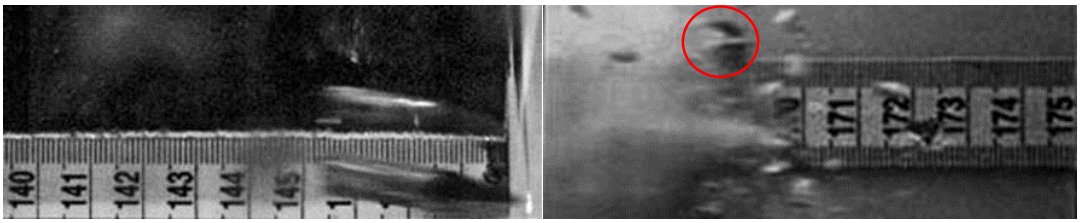

Figure 4. HSV view of incoming round (left) and exiting round (right)

Figure 5 shows a photo of the experimental set-up with the two overhead HSV focused on the pink alumina tile. The image on the right shows the bullet from Test 13 that was recovered from the bullet catcher. The tip of the bullet is missing which is the case for all post-test bullets. The jacket remains largely intact and in most cases slipped forward on the penetrator leaving the end cap detached. In most cases, the lead tip used for bullet stability, was missing/not found.

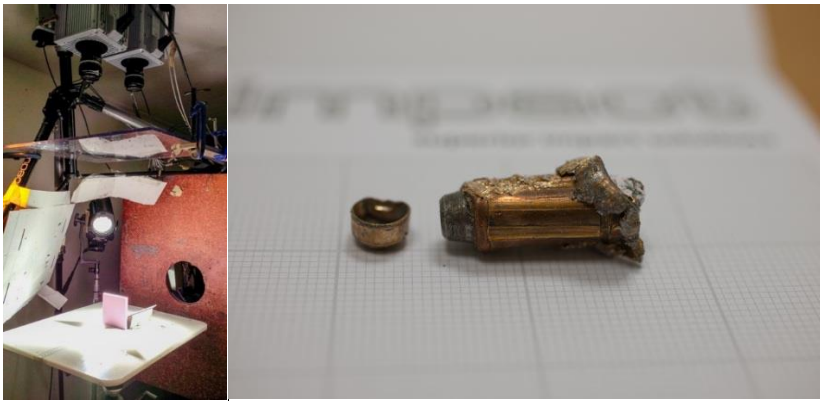

Figure 5. Experimental set-up prior to test (left) and typical bullet (Test 13) deformation (right)

Table 2 lays out the results. This includes the calculated yaw, impact velocity and ΔV. Tests: 2, 3, 6, 7, 11, 13, 16 and 18 were considered for the study. Tests: 1, 8, 12, 17 and 21 are not presented due to issue with HSV recording.

Table 2. AP M2 tests and calculations from HSV

Test ID	Yaw	Impact Velocity	ΔV
	[°]	[m/s]	[m/s]
2	13.0	514	189
3	4.0	497	278
4	9.9	511	272
5	0.0	760	149
6	10.5	381	260
7	2.7	655	207
9	8.5	495	244
10	15.6	486	279
11	12.3	424	248
13	9.9	494	207
14	4.0	472	228
15	12.7	487	256
16	12.0	494	253
18	6.6	520	223
19	5.1	460	231
20	11.2	495	199

Figure 6 shows the graph of ΔV vs. Yaw angle. This shows a clear trend of increasing velocity change (ΔV) with Yaw angle. The linear trend line indicates increased armour effectiveness with increased yaw as one would expect. The polynomic trend line suggests relatively low velocity loss for yaw angles around 12º. However, the small sample size does not include evidence of tests with yaw showing less velocity loss than the no yaw scenario.

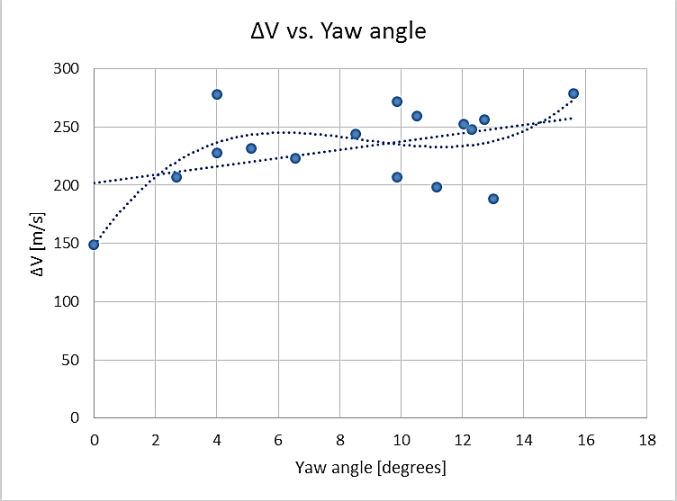

Figure 6. ΔV vs. Yaw (Experiments)

Figure 7 shows a graph of the measured ΔV as a function of the Impact velocity. The trend line indicates reduced effectiveness of the armour at higher impact speeds.

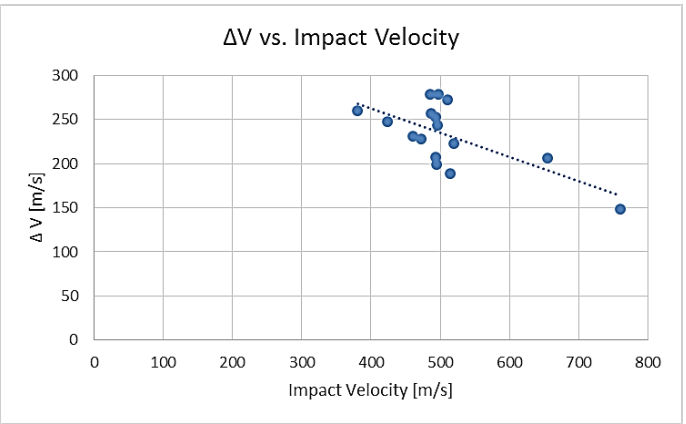

Figure 7. ΔV vs. Impact Velocity (Experimental)

4. FINITE ELEMENT MODEL

The finite element model of the assembly consists of Threat (30-06 7.62 x 63mm AP M2) and Target (Alumina ceramic tile). The threat is made up from a combination of materials and element formulations suitable for discretisation of the part geometry described in Sec. 2 and their deformation characteristics.

The commercially available RADIOSS explicit time-integration software, provided by Altair is used for modelling of the ballistic load cases. This analysis code has been shown to be well suited in dealing with the complex material and geometric non-linearities and the multiple contact interactions that occur in this study. The RADIOSS models of the full assembly are run on a high performance Windows based computer system utilizing multiple cores. Overall model size is of the order of 5M elements and a 100 μs impact can take several days to solve. Being a time-integration solver, the smallest elements within the relatively high Young's Modulus ceramic tile control the time-step for the solution. The solution is based on a natural time-step calculation.

The finite element mesh of the threat was built from CAD data derived from CT scanning of the projectile (Sec. 2) carried out by the TSB project partners at WMG (University of Warwick). This consisted of 2D shell elements to represent the relatively thin jacket. The lead tip was represented as SPH (Smooth Particle Hydrodynamics) as this special element formulation available in RADIOSS is particularly well suited for predicting the large deformation fluid-like interaction of the lead with the other relatively hard parts of the assembly. The hardened steel penetrator is a hybrid model consisting of 3D solid elements as well as SPH particles towards penetrator's tip as this area experiences high strains which are a challenge for 3D elements to handle. A set of elastic-plastic isotropic material models is used to define the threat components. Their properties have been derived from literature [6] and validated in a correlation process making use of a series of drop tests where a mass is dropped onto the threat was constrained at the base and standing upright.

The finite element mesh of the simple prismatic ceramic target is made up of 3D brick elements 0.25 mm x 0.25 mm x 0.25 mm giving 32 bricks through thickness. This results in a very detailed representation of the ceramic tile which is required to capture the known failure mechanism. A Johnson-Holmquist constitutive model was selected to represent the brittle failure response of the alumina ceramic and the parameters have been derived from literature [7] [8] [9] [10], Split Hopkinson Bar experimental testing and series of ballistic tests.

Figure 8 shows the typical model set-up where the threat is positioned against the target at t=0. The threat is given an initial velocity as measured in test along the X axis. A rigid wall is used to support the tile and represents the experimental set-up described in Sec. 3. Acceleration due to gravity is included in the simulation. Bullet rotation was not assumed. This has been investigated but was found to have a negligible effect therefore, for modelling simplicity, it is not included in the results presented.

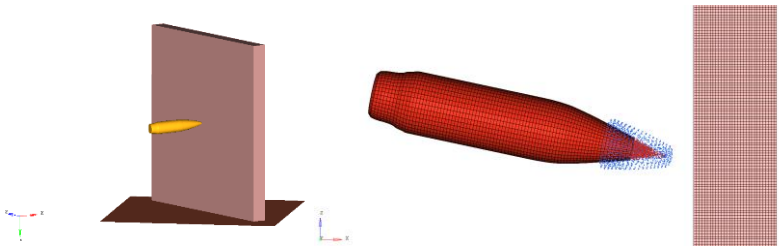

Figure 8. RADIOSS finite element model of the assembly including the yawing AP M2 (left) and close up of penetrator with SPH lead tip and ceramic tile (right)

4.1 FEA results

The FEA model was utilised to simulate a selection of the total number of tests in order to identify the system conditions responsible for the observed phenomenon that yaw can reduce the armour effectiveness. **Table 3** shows the results that were generated with the FEA models. Tests 6* and 11* were simulated to investigate target response locally at impact point therefore were not simulated until complete round penetration and ΔV could not be measured.

Table 3. Results with FEA Model Delta V

Model ID		5	6	6*	7	10	10*	11	11*
Yaw	[°]	0	10	10	3	16	0	12	12
Impact Velocity	[m/s]	760	381	424	655	486	486	424	381
ΔV	[m/s]	148	241	-	161	262	195	200	-

Figure 9 shows the simulation results overlaid in red on the results from the experiments. There is a good correlation between the developed FEA model and experimental test for the non-yaw Test 5. The scenarios with yaw show a smaller ΔV in the simulation. However, the trend of reduced armour effectiveness for yaw angles around 12° was replicated. This justified the use of the simulation results to investigate the phenomenon with caution.

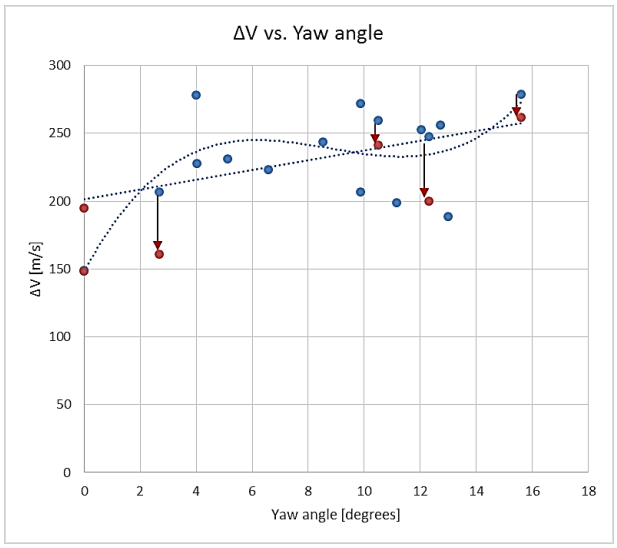

Figure 9. ΔV vs. Yaw Angle for Experiment (in blue) and FEA Model (in red)

5. OBSERVATIONS & ANALYSIS

In this section, visual results are presented from the FEA model. A numerical model allows one to review a multitude of results in a highly visual way. This includes contour pressure plots which show the propagation of wave fronts and these can be generated in any plane by taking cross sections of the alumina.

Figure 10 shows the back face of the reassembled target post-test and corresponding FEA mode at 125 µs. Note that at 125 µs the cone shaped group of fragments in the model obstruct the view of the fracture surface that is visible on the reassembled target post-test. However, the contour is clearly visible.

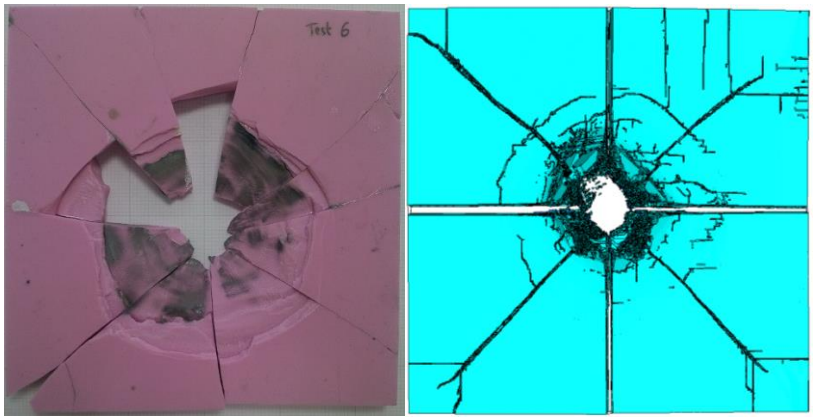

Figure 10. Back-to-back comparison between reassembled target and simulation results (Test 6)

A series of Hopkinson bar experiments carried out on prismatic samples made of 95% Al_2O_3 prior to this study has shown that above certain impact velocity of the Hopkinson bar the sample splits approximately half-way across its length. The impact velocity in these experiments is directly proportional to the magnitude of the pressure wave generated in the sample. The tensile pressure, also referred to as spalling pressure, is believed to be one of the main failure mechanisms which occur in a high speed impact. It is thought that the circular plug ejected from the back face of the alumina tile is created in a similar way. Pressure results are one of many which can be looked at in a finite element model.

Test 10 (with a resultant yaw of 15.6º) has been re-run at the same velocity with the threat having no yaw giving Test 10* and enabling a direct comparison of results. **Figure 11** shows a pressure contour plot taken at a horizontal cross section of the target and compares the propagation of a negative pressure wave for a non-yawed and yawed round. Clearly visible is the pressure front

advancing faster through the thickness for the yawing round. A thin layer of elements are eroded directly behind this wave front in the model resulting in a radial horizontal crack. This radial crack can also be found in the vertical section which is the straight blue line in each of the subsequent images below. At 4µs the pressure front has already arrived at the back face of the target in the case of the yawing round.

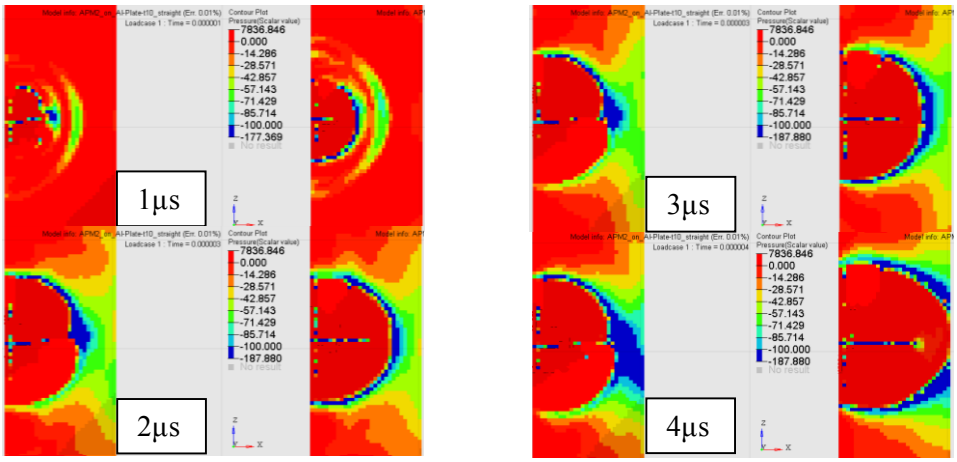

Figure 11. Comparison of negative pressure front propagation through the thickness between non-yawed (left) and yawed (right) threat impacting at the same velocity.

Figure 12 shows through-thickness comparison of the non-yawed and yawed scenarios, Test 10* and Test 10 respectively, and their subsequent damage sequence up to 30 µs. The images shown are made transparent with feature lines. The occurring shapes are eroded elements which are damaged effectively showing the amount of damage inside the target tiles. The comparison suggests the yawed threat causes a more centralised continuous damage to the target. Also, initially at approximately 15 µs the comparison shows a significant unsymmetrical damage.

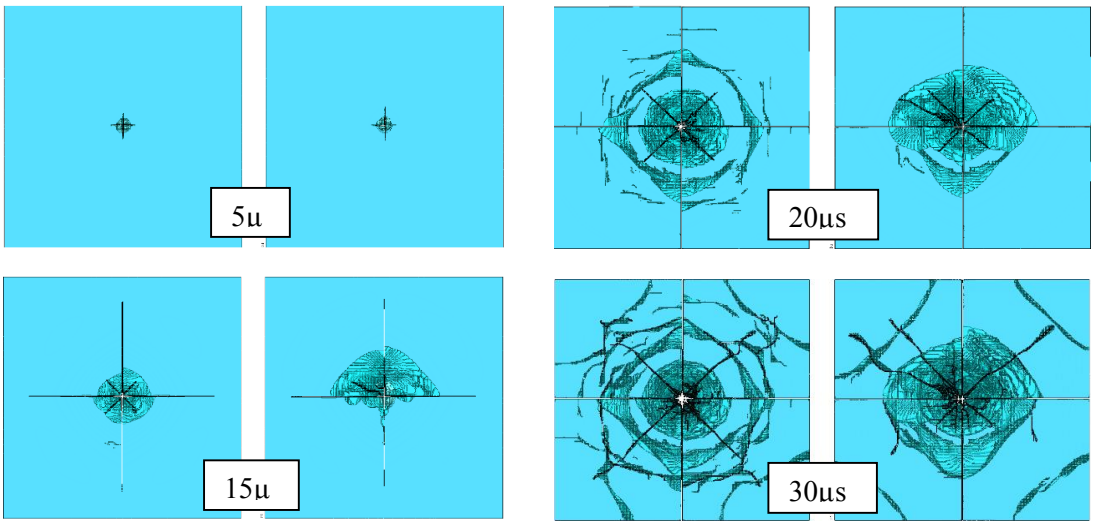

Figure 12. Comparison of through-thickness damage propagation between non-yawed (left) and yawed (right) threat impacting at the same velocity.

Test 11 happened to fall in the Yaw range of relatively low ΔV. In the numerical study, Test 6 was re-run at the velocity of Test 11 (424 m/s) to give a direct comparison of modelling results for the different yaw angles.

Figure 13 shows a horizontal cross section of the model taken at the tip of the bullet at 6 µs. This shows the erosion of the front face of the ceramic and the development of the vertical crack. In Test 6, the crack has not developed to the rear face of the ceramic tile whereas at the same time, it has in the case of Test 11.

Figure 14 shows the back face of the ceramic at 8 µs. Asymmetry of the crack propagation is observed in Test 11 where the horizontal crack has not yet developed to the back face of the ceramic.

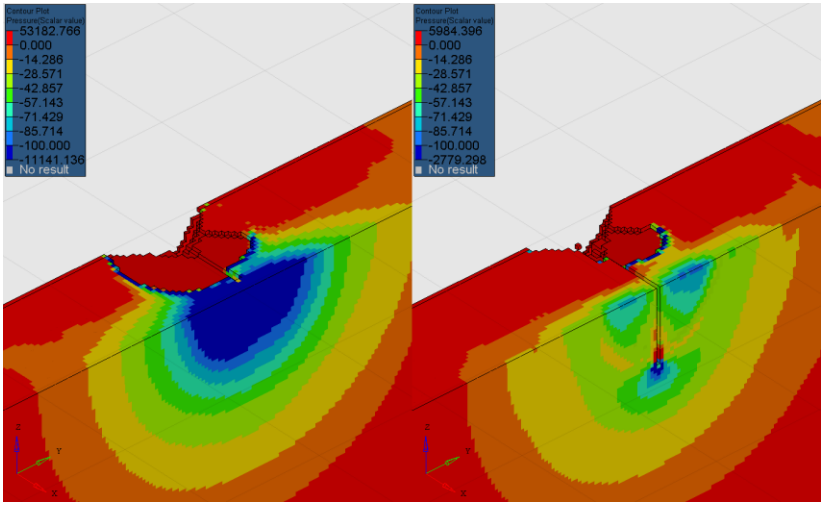

Figure 13. Horizontal cross section through Test 6 (left) and Test 11 (right) models at 6µs.

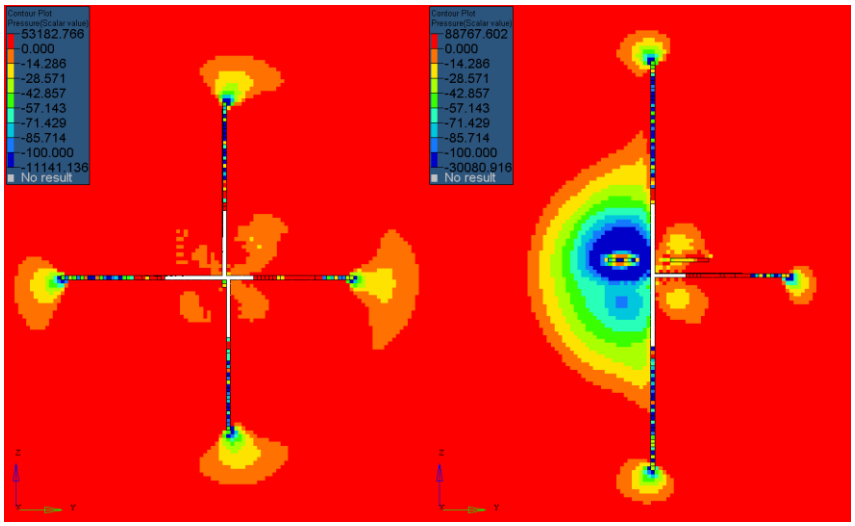

Figure 14. Assymetric cracking and pressure disrribution on the back face of the ceramic model (Test 6 on the left and Test 11 on the right).

6. CONCLUSIONS

- Finite element analysis is suitable for this type of analysis due its capabilities giving more insight into component response and behaviour. It has an advantage over physical testing as far as visualisation and hence understanding of the impact events is concerned.
- The Finite element model used for this study shows similar ΔV vs. Yaw angle trend though ΔV is under-predicted in general when compared to test results.
- Generally, yawed bullets experience higher ΔV than non-yawed bullets. This suggest higher armour effectiveness in case of a yawed threat impact assuming armour effectiveness is directly proportional to decrease of threat velocity.
- More centralised continuous damage to the target is observed for a yawed impact when non-yawed and yawed impacts at similar velocities are compared. A more centralised damage suggests that not all of the target is involved in consuming the impact energy.
- Assuming an ideal perpendicular impact with no yaw, the bullet only exerts a force on the target in the direction of travel. In a scenario where the threat yaws upon impact, the bullet develops a tangent force component as well. At the same time however, the threat will rotate and therefore use some of its kinetic energy for rotation. Although a yawed bullet carries less kinetic energy, the tangent force component is developed which can still contribute to the damage to the target.

- Higher negative pressure front velocity for a yawed than non-yawed bullet suggests the damage in a yawed impact propagates quicker through the thickness. The faster propagation of the negative pressure could be related to the larger contact force.
- For the investigated bullet and armour combination, the kinetic energy reduction as a result of rotation appears to not outweigh the tangent force component effect for yaw angles around 12 degrees.

Acknowledgements

The authors would like to thank Jay Jeffs from Morgan Advanced Materials for his help in setting up and carrying out the experimental tests. Also, we would like to thank David Lemouton from Simpact Engineering for his contribution in in processing the experimental test results and setting up the CAE models for solving.

References

[1] Watson, C.H.; Bates, L.; Horsfall, I. The effect of low-angle yaw on the armour penetration of light armour-piercing projectiles. Journal of Battlefield Technology Vol. 13, No. 3, November 2010.
[2] Hazell P.J., Iremonger M.J., Barton P.C., Broos J.P.F. Anomalous target failure at small angles of obliquity. Proceedings of the 21st International Symposium on Ballistics, Adelaide, Australia, 19-23 April (2004).
[3] Gotts, P.; Tawell, M.; Holden, S. Variations in ammunition used for testing personal armour. Proceedings of the Personal Armour Systems Symposium, 2010.
[4] Kumar J. et al, Inconsistency in 9mm bullets measured with non-destructive X-ray computer tomography, Forensic Sci. Int., 214 (2011), 48-58.
[5] Thornby J. et al, Inconsistency in 9 mm bullets: Correlation of jacket thickness to post-impact geometry measured with non-destructive X-ray computed tomography, Forensic Sci. Int., 234 (2014), 111-119.
[6] Flores-Johnson E.A. et al, Ballistic performance of multi-layered metallic plates impacted by a 7.62-mm APM2 projectile, International Journal of Impact Engineering, Vol. 38, Issue 12, December 2011, 1022-1032.
[7] Klasztorny M. et al, Numerical modelling and design of ALFC shield loaded by 20mm FSP fragments, Journal of KONES Powertrain and Transport, Vol. 19, No. 4 (2012).
[8] Zhang X. et al, Numerical study on penetration process of multi-layer ceramic target by shaped charge jets, Proceedings of ICMEM2007, International Conference on Mechanical Engineering and Mechanics, November 5-7, 2007, Wuxi, China.
[9] Zhan-Feng S. et al, The spall strength and shock compressive damage of AD95 ceramics, Acta Phys. Sin., Vol. 61, No. 9 (2012) 096201.
[10] Zhan-Feng S. et al, The response of AD95 Alumina to low pressure impact, International Journal of Nonlinear Sciences & Numerical Simulation, 11, 247-251 (2010).